Geomechanics and Engineering, *Vol. 29, No. 4 (2022) 435-449*
https://doi.org/10.12989/gae.2022.29.4.435

Discrete element modeling of strip footing on geogrid-reinforced soil

Vahab Sarfarazi*[1], Abdollah Tabaroei[2a] and Kaveh Asgari[3b]

[1]*Department of Mining Engineering, Hamedan University of Technology, Hamedan, Iran*
[2]*Department of Civil Engineering, Eshragh Institute of Higher Education, Bojnourd, Iran*
[3]*Department of Mining Engineering, Shahid Bahonar University of Kerman, Kerman, Iran*

(Received December 17, 2021, Revised February 22, 2022, Accepted March 9, 2022)

Abstract. In this paper, unreinforced and geogrid-reinforced soil foundations were modeled by discrete element method and this performed under surface strip footing loads. The effects of horizontal position of geogrid, vertical position, thickness, number, confining pressure have been investigated on the footing settlement and propagation of tensile force along the geogrids. Also, interaction between rectangular tunnel and strip footing with and without presence of geogrid layer has been analyzed. Experimental results of the literature were used to validation of relationships between the numerically achieved footing pressure-settlement for foundations of reinforced and unreinforced soil. Models and micro input parameters which used in the numerical modelling of reinforced and unreinforced soil tunnel were similar to parameters which were used in soil foundations. Model dimension was 1000 mm* 600 mm. Normal and shear stiffness of soils were $5*10^5$ and $2.5*10^5$ N/m, respectively. Normal and shear stiffness of geogrid were $1*10^9$ and $1*10^9$ N/m, respectively. Loading rate was 0.001 mm/sec. Micro input parameters used in numerical simulation gain by try and error. In addition of the quantitative tensile force propagation along the geogrids, the footing settlements were visualized. Due to collaboration of three layers of geogrid reinforcements the bearing capacity of the reinforced soil tunnel was greatly improved. In such practical reinforced soil formations, the qualitative displacement propagations of soil particles in the soil tunnel and the quantitative vertical displacement propagations along the soil layers/geogrids represented the geogrid reinforcing impacts too.

Keywords: geogrid; footing settlement; PFC 2D; strip footing

1. Introduction

Geogrids have significant strength and toughness, and because of this fact can be used as an effective and frugal way to strengthen unconfined granular materials and have been greatly used in geotechnical engineering (Zhang 2013, Yang 2012, Indraratna 2011). Geogrids have shown great results in strengthening the railway embankment; in addition geogrids with suitable apertures can significantly control the lateral deformation and ballast degradation of the track bed (Sweta 2019, Ngo 2014, Biabani 2016, Indraratna 2013). Many investigators have performed several experimental (Esmaeili 2017, Qian 2018, Teixeira 2007, Nimbalkar 2014, Han 2018) and theoretical (Lu 2006, Miao 2017, Ngo 2016, Gutierrez 2015, Allen 2018, Bathurst 2017a, b, Bathurst 2019, Lin 2018a, b) researches to investigate the interaction mechanism between geogrids and ballast particles and examine the important role of geogrids on the overall ballasted track performance. All results of these researches indicated that geogrid has a good effect in the stability of ballast bed; in addition, it was shown that the mechanical and physical properties of distinct particles greatly affect the behavior of ballast under both static and dynamic loading. The strength of the granular material influenced by not only the grain or the geogrid distinct characteristics but on the accordance between aperture size and particle size (Brown 2007, Miao 2017, Gu 2016, Yaylaci 2013, Yaylaci 2016, Uzun Yaylacı 2020, Öner 2015, Adiyaman 2015). The interaction mechanism between geogrid and the ballast consists of the interface abrasion and the ribs limitation on the particles. In the case of coarse-grained reinforcement system, the limitation effect has a more important impact (Indraratna 2012). Several investigators examined the optimal ratio between ballast particle size and aperture size. McDowell *et al.* 2006, considered the peak interface strength as an index to investigate the accordance between the ballast diameter and the biaxial geogrid aperture (rectangular apertures) size, results showed that for a ballast compound with a diameter of 40 mm, for obtaining the optimal strength ratio of aperture size to ballast diameter should be 1.4. Other researchers such as Brown *et al.* 2007 examined the interlocking effect between geogrid and ballast and mechanical behavior and indicated that the optimal ratio of the rectangular aperture size to the ballast size is 1.2–1.6. Ngo *et al*. 2017, Han *et al*. 2018, compared results of large-scale direct shear experiments and numerical simulations with biaxial geogrids and triaxial geogrids, they indicated that increasing the number of ribs connected to a single joint (Dong 2011) results in higher shear strength of interface and more consistent stiffness. Considering results

∗Corresponding author, Ph.D.
E-mail: Sarfarazi@hut.ac.ir
[a]Assistant Professor
E-mail: a.tabaroei@eshragh.ac.ir
[b]Research Scholar
E-mail: kavehaskary1373@gmail.com

ISSN: 2005-307X (Print), 2092-6219 (Online)

Table 1 Experimental factors of sand and geogrid (Das *et al*. 1994)

Silica sand	
Dry unit weight (kN/m^3)	17.14
Particle sizes d (mm)	0.2-0.85, d_{50}= 0.48
Relative density (%)	70
Friction angle (°)	41
Biaxial geogrid (Tensar BX1000)	
structure	17.14
Aperture size MD/XMD (mm)	0.2-0.85, d_{50}= 0.48
Nominal rib thickness (mm)	70
Nominal junction thickness (mm)	41
Tensile stiffness at 2% strain (kN/m)	182

of a series of experimental and numerical pull-out tests, Chen *et al*. 2018, indicated that under similar situation the geogrid with 70 mm triangular apertures in comparison to the geogrid with 65 mm square aperture for the ballast with 40 mm diameter is more operative. Most of recent studies used biaxial geogrids or D_{50} (average particle size) to recognize the optimal ratio relationship between aperture and aggregate particle. Although D_{50} is just a grading index of particle size, and can't clearly represent the cooperation of the optimal particle size to the reinforcement accomplishment (Han 2018). The range of D_{50} also includes some particles that are too coarse or too fine, these particles afford higher strength and less settlement (Choudhary 2016) while, and they have little collaborate in interlock between geogrid and grains. Thus, considering the synergy between geogrid and ballast, for identifying the coordinative relationship between aperture size and ballast diameter, solo-sized particles are more appropriate (Brown 2007). In addition, geogrids with triangular aperture properties have been greatly considered to strengthen different unconfined granular aggregates. Accuracy of measurement limited the Experimental investigations and performing absolute single-sized particles for laboratory tests is difficult. In other hand, Alternatively, the commercial software Particle Flow Code based on DEM in two/three dimensions has been applied by several investigators to identify the mesoscopic mechanical response and fundamental behavior of granular assembly (Thornton 2000, Lin 2020, Lin 2021 a, b, Dong 2020, Mcdowell 2002, Zhao 2002, Wang 2016, Miao 2017, Gao 2018, Wang 2014, Das 1994, Tran 2015, Huang 1990, Chen 2007, Demir 2014, Wang 2020, Khing 1993, Kim 2020, Luat 2020, Yang 2018, Moradi 2019, Rezaei 2019, Yaylaci 2020, Yaylaci 2021a, b). In this study, the effect of horizontal position of geogrid, vertical position, thickness, number, confining pressure have been investigated on the footing settlement and tensile force propagations along the geogrids. Also, the interaction between rectangular tunnel and strip footing with and without presence of geogrid has been analyzed.

2. Experimental background

Numerical modeling of this research was validated by results of Das *et al*. (1994), investigation about the unreinforced and reinforced soil structures under surface strip footing loads. Table 1, shows the experimental factors of geogrids and sand. Additional data of the sand and geogrid characteristics can be seen in the papers (Das *et al.* 1994). The unreinforced and reinforced soil foundations were built from multilayers, and the thickness of each layer was 25 mm. In case of reinforced foundations, the depth of top geogrid layer was nearly 25mm under the surface of soil. For the case reinforced with multiple geogrid layers, the vertical distance between two close geogrid layers was also 25 mm. Each geogrid layer had a length of 762 mm. Then, the final soil layer had been placed in each sample and the soil surface was covered by a strip footing. A registering ring and two dial gauges were measured the induced vertical load and the corresponding footing settlement, respectively.

3. Numerical modeling of geogrid reinforced soil foundation

In this research, PFC 2D used in discrete element modeling to evaluate the geogrid–soil interaction under surface strip footing loads. The linear contact stiffness and contact bond model were used to modelling the soil (Fig. 1(a)). The bonded particles modelled the geogrid. High knots were placed at the position of the connection points so that the contributions of geogrid transverse members could be simulated. Thus, the knot particles were able to transmit the bearing resistances due to the transverse members in these two-dimensional researches to the longitudinal parts (Wang *et al*. 2014. In this investigation, dimension of geogrids and the numerical soil were different compared to laboratory samples (Das *et al,* 1994). Since the strip footing was loaded symmetrically on the soil, numerical sample was simplified into half of the physical sample so that the DEM simulation results during reasonable computational time were provided. Fig. 1 depicted the reinforced soil sample loaded with a strip footing, in which bonded particles was modeled the strip footing and it was possible to induce the vertical loads using a horizontal wall onto the bonded particles. The DEM researches in this investigation focused on two major cases, i.e., simulations with and

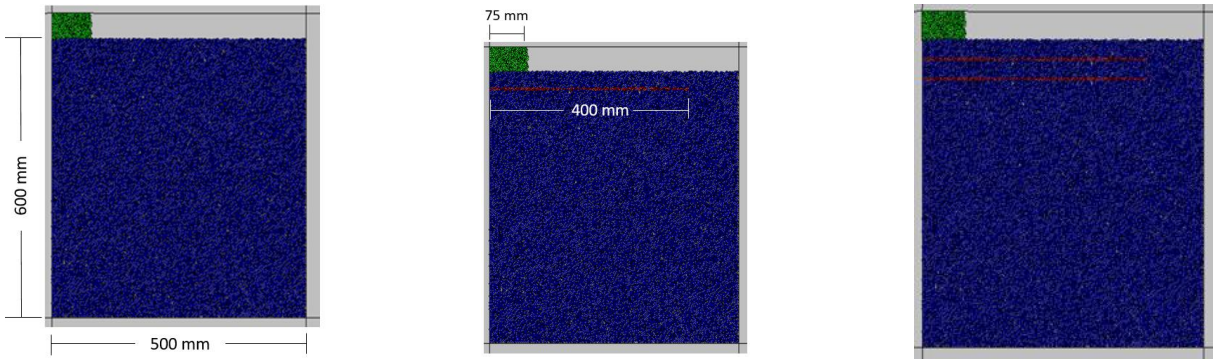

(a) (b) (c)

Fig. 1 (a) Unreinforced soil sample loaded with a strip footing, (b) reinforced soil sample with one geogrid and (c) reinforced soil sample with two geogrids

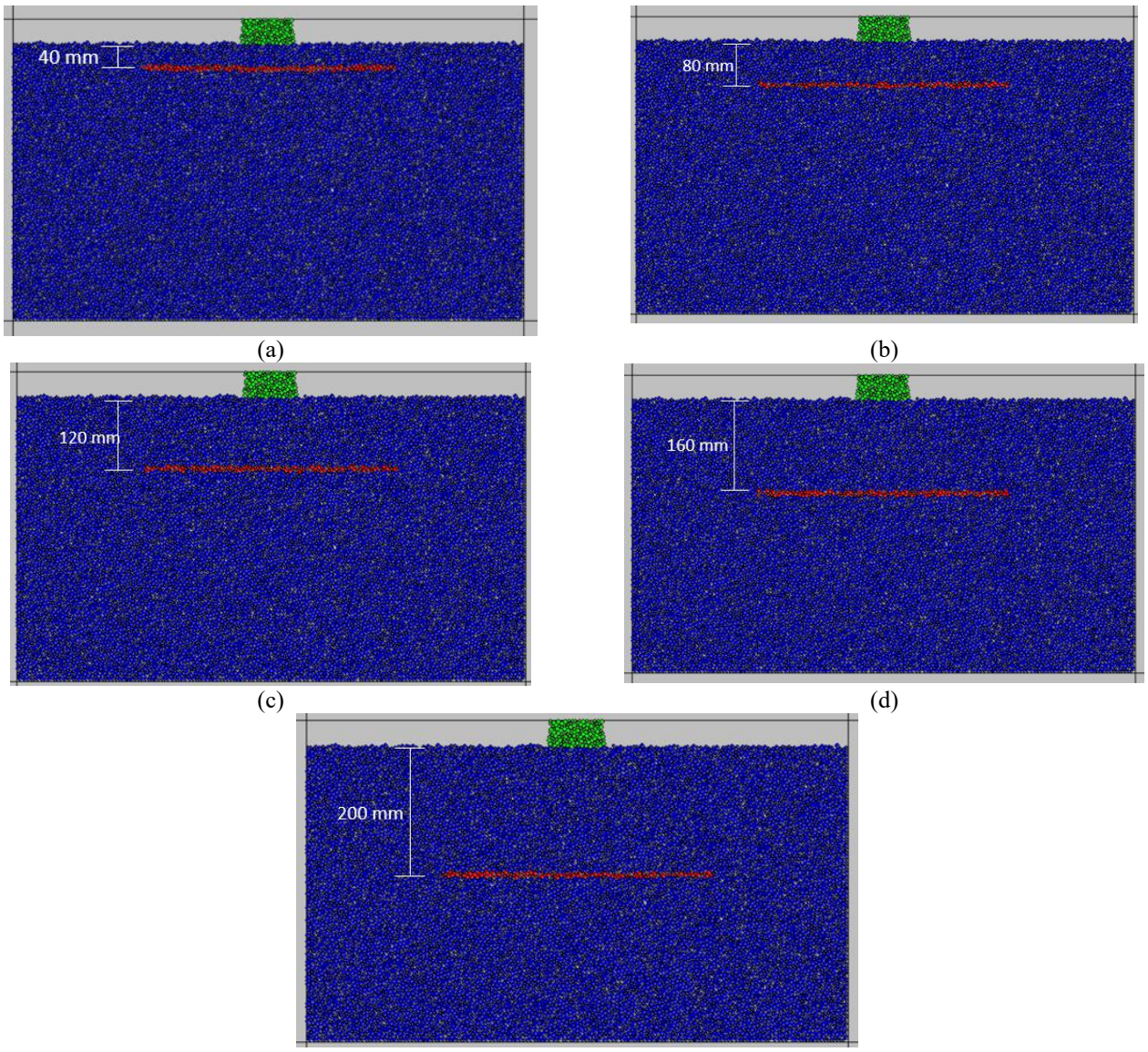

(a) (b) (c) (d) (e)

Fig. 2 Vertical distance between one geogrid and strip footing was (a) 40 mm, (b) 80 mm, (c) 120 mm, (d) 160 mm and (e) 200 mm

without presence of confining pressure. In the absence of confining pressure, the investigations focus on the cases of unreinforced (N=0 in Fig. 1(a)), reinforced with one geogrid layer (N=1 in Fig. 1(b)) and reinforced with two

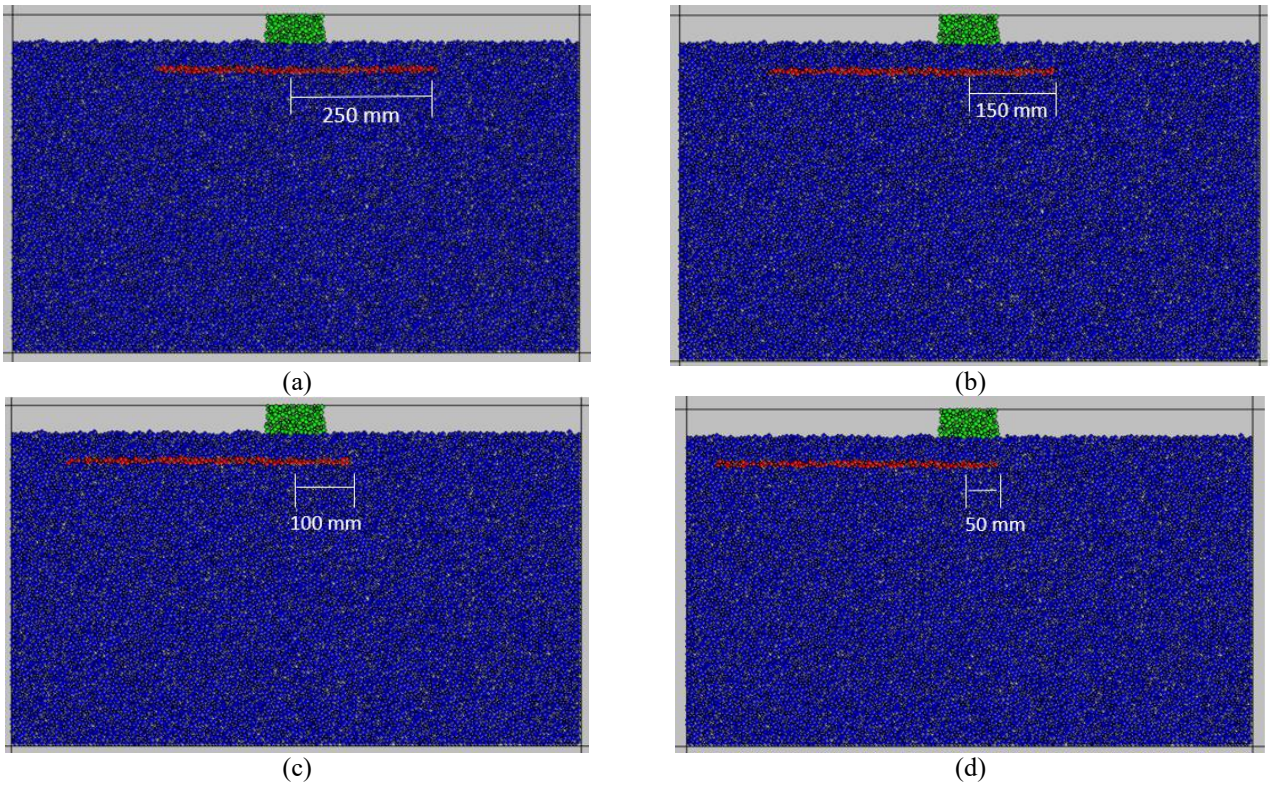

(a) (b) (c) (d)

Fig. 3 Horizontal distance between right edge of geogrid and center of strip footing was; (a) 250 mm, (b) 150 mm, (c) 100 mm and (d) 50 mm; vertical spacing between geogrid and footing was kept constant 40 mm

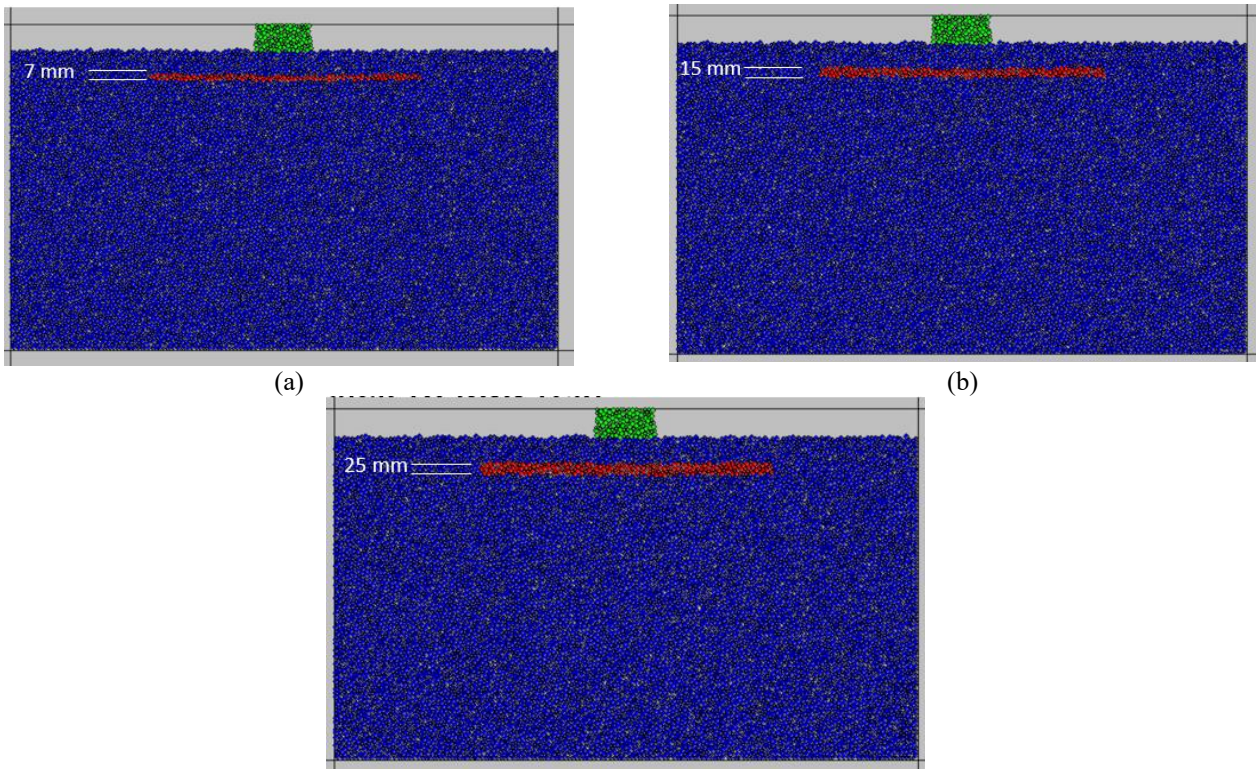

(a) (b) (c)

Fig. 4 Geogrid thickness was; (a) 7 mm, (b) 15 mm and (c) 25 mm; vertical spacing between geogrid and footing was kept constant 40 mm

geogrid layers (N=2 in Fig. 1(c)). The length of the numerical soil samples was 500 mm and their height was 600 mm. The width of the strip footing in numerical analysis was 75 mm. Each numerical sample included five

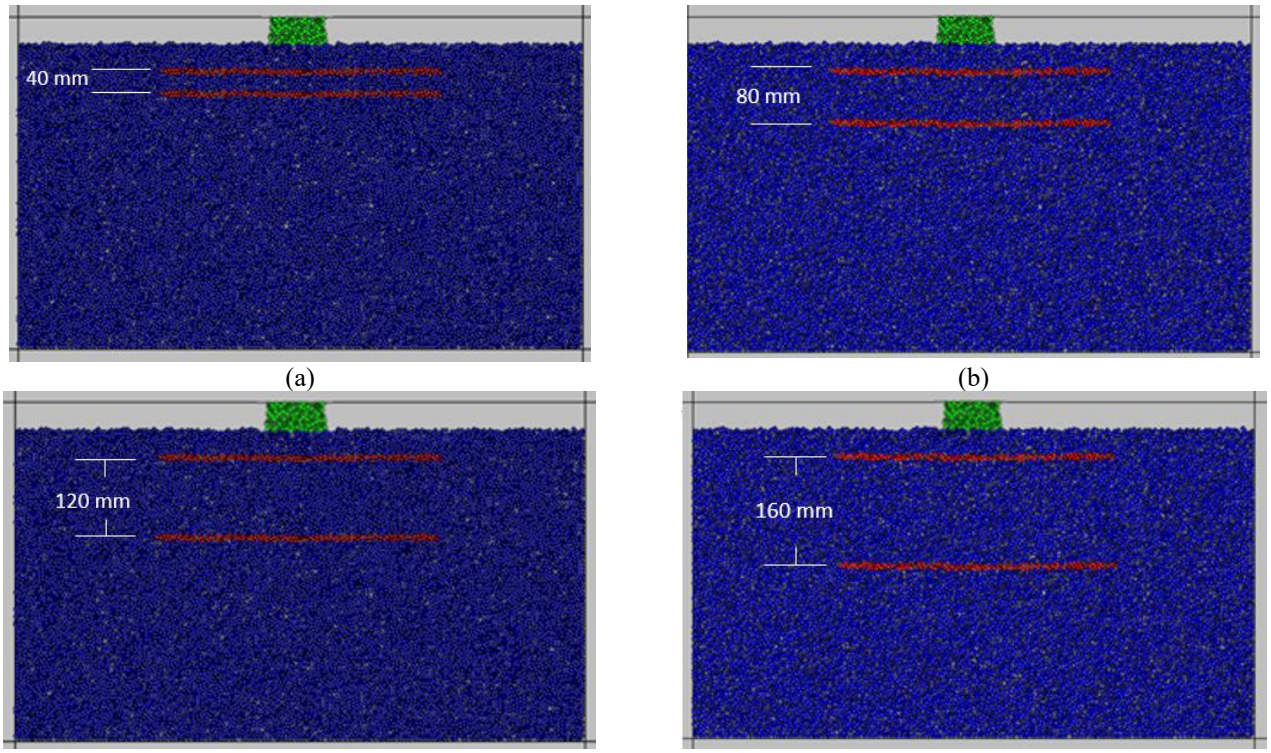

Fig. 5 Vertical distance between two geogrid was (a) 40 mm, (b) 80 mm, (c) 120 mm and (d) 160mm; vertical spacing between upper geogrid and footing was kept constant 40 mm

soil layers (two top layers and five bottom layers), as well as, the thickness of each bottom and top layer was 100 mm and 50 mm, respectively. Thus, at corresponding locations, when the reinforced samples were N=1 and N=2 (as shown in Fig. 1) it was possible to use the geogrid layers with lengths of 400 mm. The maximum of the equilibrium state of each soil layer happened when the contact force ratio reached 0.001. As the final soil layer had been provided in the soil sample, to model the strip footing a set of bonded particles were produced on the soil surface. A vertical pressure of 10 kPa with an increasing range, was directly applied to the bonded particles till the numerical samples were failed. For all loading steps, when the ratio of the maximum unbalanced force to the maximum contact force in the sample decreased below 0.001, equilibrium state was provided. Pending process of loading and in at equilibrium state of each loading step, the applied vertical pressure, and consequent footing settlement were recorded. In addition, the tensile forces, and vertical displacements along the geogrids in the case of the geogrid reinforced soil foundations, were recorded. In the presence of confining pressure, the investigations focus on the cases of reinforced with one geogrid layer (geogrid vertical position (Fig. 2) and geogrid horizontal position (Fig. 3), geogrid thickness (Fig. 4), reinforced with two geogrid layers (N=2) (geogrid vertical position (Fig. 5), reinforced with three geogrid layers (N=3) (geogrid vertical position (Fig. 6). Each individual numerical sample was composed of five soil layers (two top layers and five bottom layers), as well as, the thickness of each bottom and top layer were 100 mm and 50 mm, respectively. Thus, it was possible to place the geogrid layers with lengths of 500 mm at corresponding locations, when the reinforced cases were N=1, 2 and 3 (as shown in Figs. 2-6). The equilibrium state of each soil layer reached the maximum value as the contact force ratio was 0.001. To model the strip footing a set of bonded particles were produced on the soil surface, after the final soil layer had been provided in the soil sample. For each loading step, equilibrium state was provided when the ratio of the maximum unbalanced force to the maximum contact force in the sample decreased below 0.001. Pending the loading process and in at the equilibrium state of each loading step, the applied vertical pressure, and the resulting footing settlement were recorded. In addition, the tensile forces, and vertical displacements along the geogrids in the case of the geogrid reinforced soil foundations, were recorded. These experiments were performed under four various confining pressures i.e., 0.001 MPa, 0.005 MPa, 0.01 MPa and 0.05 MPa. In the numerical investigations width of the strip footing was 100 mm (Figs. 2-6). Height and length of the numerical soil samples were 600 mm and 1000 mm (Figs. 2-6). Loading rate was 0.001 mm/sec.

3.1 Validation of numerical simulation results

In this research, for the unreinforced case, first the micro input factors were calibrated to provide suitable PFC 2D simulation results were provided and compare it with the reported experimental data. Then, the reinforced case with one geogrid layer was calibrated. The experimental results in Fig. 7 compared with the numerically provided footing pressure–settlement relationships using the final input

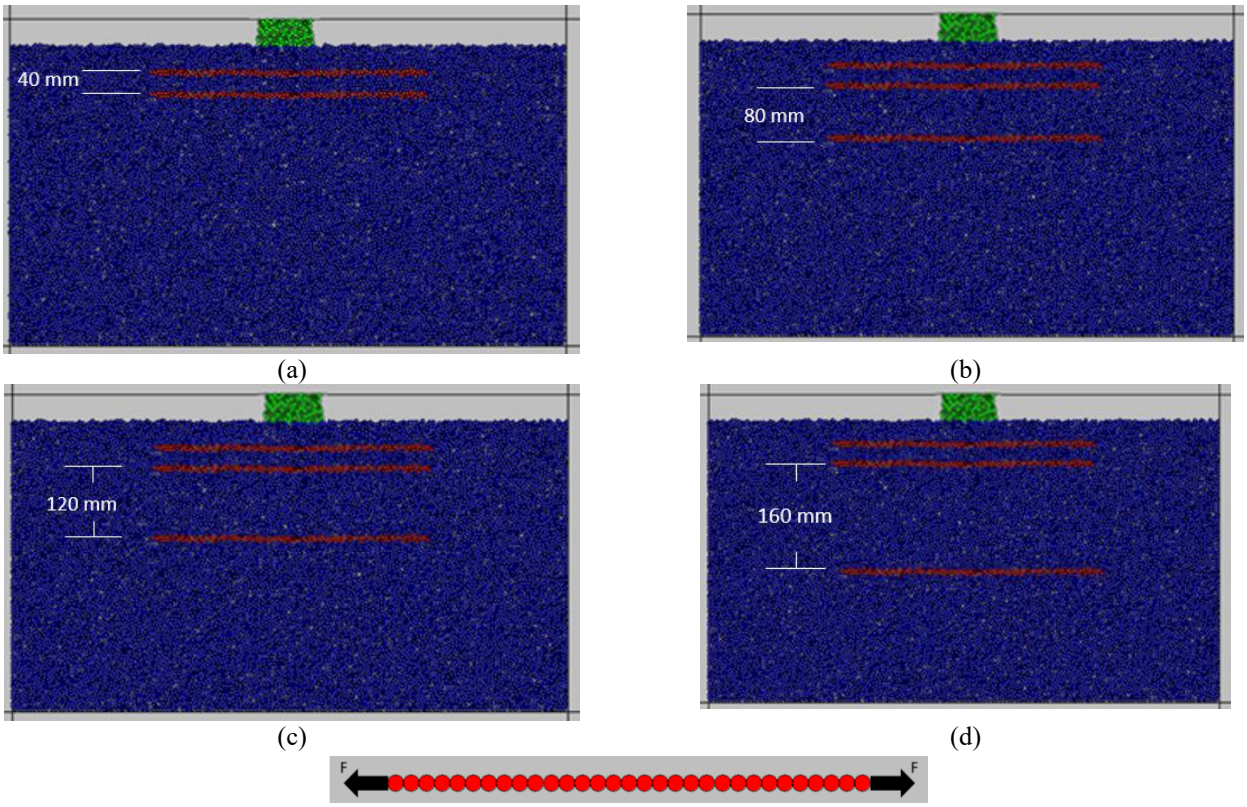

Fig. 6 Vertical distance between middle and lower geogrid was (a) 40 mm, (b) 80 mm, (c) 120 mm and (d) 160 mm; vertical spacing between upper geogrid and was kept constant 40 mm and (e) geogrid tensile test

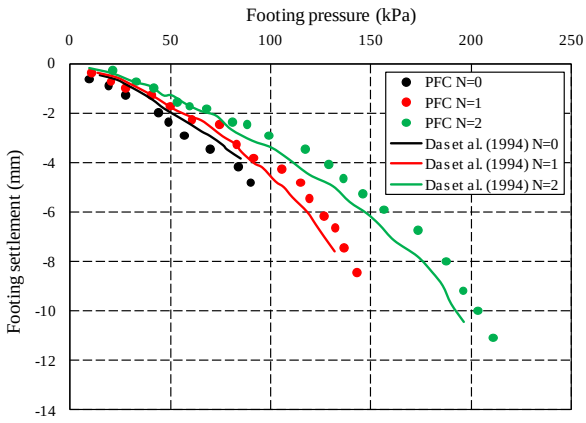

Fig. 7 Footing pressure–settlement relationships in experimental and DEM researches

factors showed in Table 2 and similar micro input factors of the geogrids (Table 3). The geogrid was represented by a cluster of balls with parallel bonds that meet the requirements of the force-displacement law. The micro-parameters of the geogrid was determined via the bolt pull-out test by try and error, as shown in Fig. 6(e). It should be considered that the soil particles in the DEM researches in this investigation were up-scaled so that during a suitable computational time, the simulation results were provided. Several previous studies used The “up-scaling” method, and the mechanical behavior of the up-scaled materials has been examined appropriately (Tran *et al.* 2015, Wang *et al*. 2014).

For the unreinforced case (N=0), the reinforced case with one geogrid layer (N=1), and geogrid layers (N=2), the DEM simulation results were well-matched with the corresponding laboratory test results. As the number of geogrids layers increased, the final bearing capacity of the soil foundation increased too. The tendency of the numerical observations was well matched with the experimental investigation results (Das *et al*. 1994). Thus, under practical loading circumstances, the current DEM models are suitable and able to evaluate the overall interaction between geogrid and soil. More DEM analyses are performed to visualize and express the geogrid reinforcement impacts.

Table 2 Input factors of soil particle, foundation particles and boundary walls

Soil particle	
Density (kg/m^3)	2650
Water content (%)	0
Normal contact stiffness (N/m)	5×10^5
Shear contact stiffness (N/m)	2.5×10^5
Normal bond (MPa)	0.04
Shear bond (MPa)	0.08
Footing particles	
Density of footing particles (kg/m^3)	2650
Minimum radius of particle (mm) / maximum radius of particle (mm)	0.25/0.415
Normal contact stiffness of footing particles (N/m)	1×10^6
Shear contact stiffness of footing particles (N/m)	1×10^6
Normal contact bond strength (MPa)	50
Shear contact bond strength (MPa)	50
Friction coefficient	0.2
Boundary walls	
Normal contact stiffness (N/m)	1×10^6
Shear contact stiffness (N/m)	1×10^6
Friction coefficient	0

Table 3 Input micro parameters of geogrid

Density (kg/m^3)	3000
Normal contact stiffness (N/m)	1×10^9
Shear contact stiffness (N/m)	1×10^9
Normal bond (MPa)	100
Shear bond (MPa)	100
Parallel bond_rad	1
Parallel bond _kn (N/m)	1×10^9
Parallel bond _ks (N/m)	1×10^9
Minimum radius of particle (mm)/ maximum radius of particle (mm)	0.25/0.415
Parallel bond _shear strength (MPa)	100
Parallel bond _normal strength (MPa)	100
Friction coefficient	0.5

As depicted in Fig. 8, The quantitative tensile force propagations along the geogrids in the reinforced samples are provided too. For each geogrid layer, the maximum tensile force was under the strip footing adjust to the symmetric boundary of the geogrid and the value decreases from the symmetric boundary to the right-side free end of the geogrid. These DEM conclusions of this research are well matched with results of laboratory test provided by Huang and Tatsuoka (1990) and Chen (2007). For the geogrid of N=1, the maximum tensile force is greater than each geogrid of N=2. For the reinforced case of N=2, the tensile forces in the upper geogrid are higher compared to the lower geogrid.

Fig. 9, shows the quantitative vertical displacements of the geogrid in N=1 and the upper geogrid in N=2. Depth of both geogrid layers in soil samples were same, i.e., 40 mm under the footing base. For better comparison, Fig. 9 shows the vertical displacements of soil particles in a horizontal

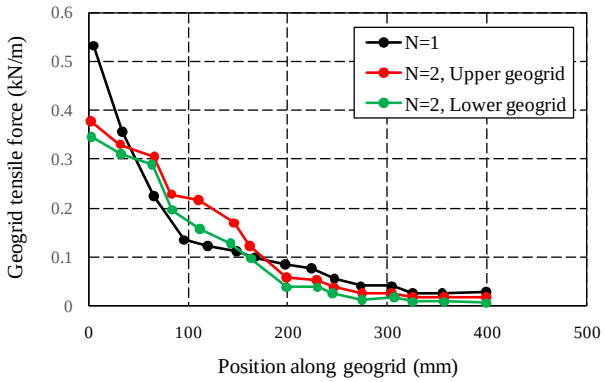

Fig. 8 Tensile force propagations along geogrid in reinforced soil samples

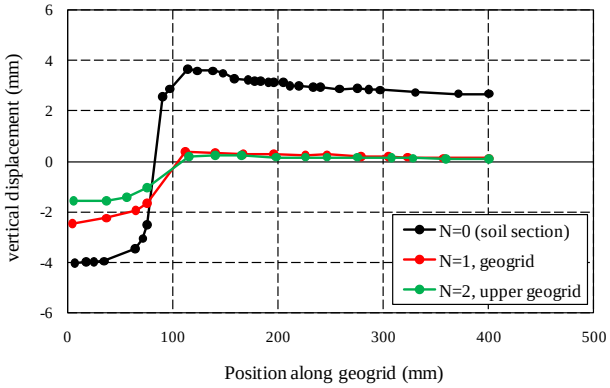

Fig. 9 Vertical displacement propagations along soil section/geogrid in unreinforced and reinforced soil foundations

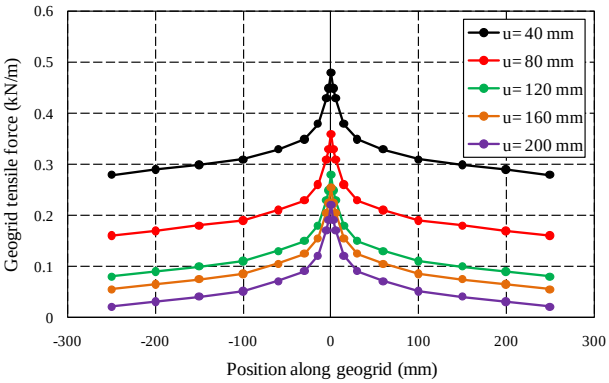

Fig. 10 Tensile force propagations along geogrid in reinforced soil specimens

part of the unreinforced case. The depth of the soil horizontal part is similar to the depths of the geogrid in N=1 and the upper geogrid in N=2. Fig. 9 indicated that the vertical displacements of the soil particles in the horizontal part below the strip footing are greatly larger than the vertical displacements along the geogrids. Outside the range of the strip footing, the soil particles have been forced aside and the vertical displacements of soil particles in the horizontal part are greater than the vertical displacements along the geogrids, although in a reverse direction (upwards). The vertical displacements along the geogrids in

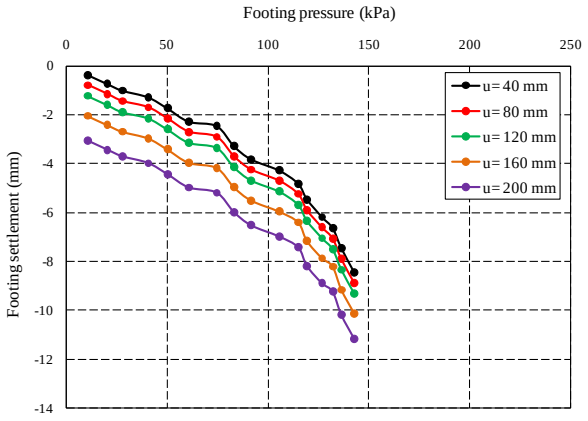

Fig. 11 Effect of geogrid spacing on the footing settlement

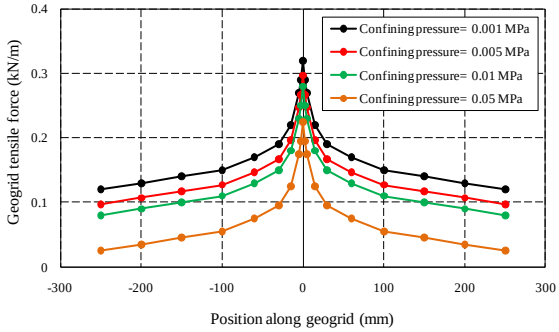

Fig. 12 Effect of confining pressure on the tensile force along the geogrids

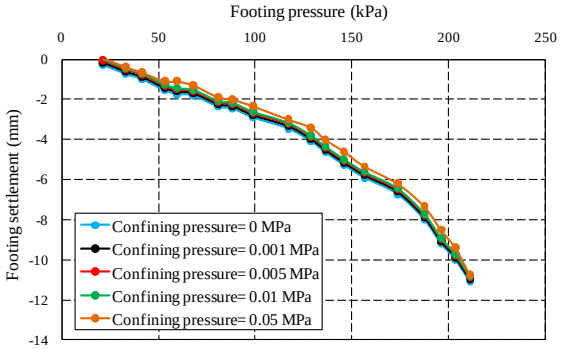

Fig. 13 Effect of confining pressure on the footing settlement

both reinforced cases were compared and it was indicated that, the vertical displacement of the geogrid in N=1 is typically greater than that in N=2.

a) The effect of vertical spacing between one geogrid and the footing on the tensile force propagations along the geogrids and vertical displacements

Effect of spacing between one geogrid and footing has been analyzed. The spacing between geogrid and footing were 40 mm, 80 mm, 120 mm, 160 mm and 200 mm (Figure 2). The tensile force propagation along the geogrids was provided, as shown in Fig. 10. It was indicated that for

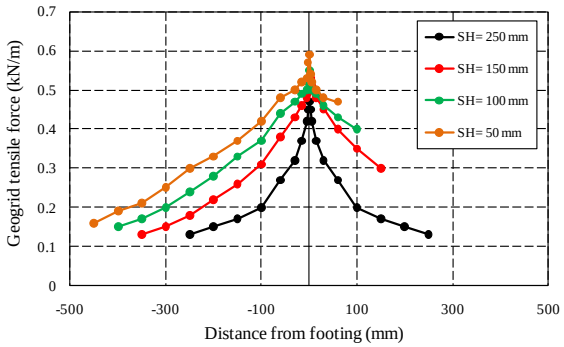

Fig. 14 Effect horizontal position of geogrid on the tensile force propagations along the geogrids

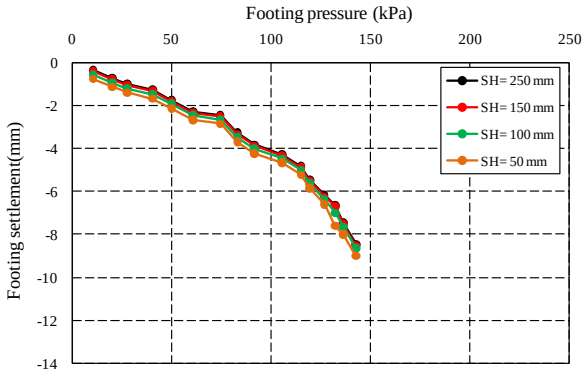

Fig. 15 Impact of geogrid position on the footing settlement

each geogrid layer, the maximum tensile force is below the strip footing and the value decreases from axisymmetric line to the both sides of the geogrid. The tensile force propagations along the geogrids were decreased by increasing the geogrid spacing.

Fig 11, shows the effect of geogrid spacing on the footing settlement. Vertical displacements along the geogrids in all reinforced cases were compared, the settlement of the footing were increased by increasing the geogrid spacing.

b) The effect of confining pressure on the tensile force propagations along the geogrids and vertical displacements

The effect of confining pressure on the tensile force propagations along the geogrids and vertical displacements for geogrid spacing of 40 mm were analyzed i.e., 0.001 MPa, 0.005 MPa, 0.01 MPa and 0.05 MPa. The number of geogrids was 1. The quantitative tensile force propagations along the geogrids were provided, as shown in Fig. 12. For each confining pressure, the maximum tensile force is found below the strip footing and the value decreases from the axisymmetric line to the both sides of the geogrid. The tensile force propagations along the geogrids were decreased by increasing the confining pressure.

Fig. 13, shows the effect of confining pressure on the settlement of the footing. Vertical displacements along the geogrids in all confining pressure cases were compared; the settlement of the footing was decreased by increasing the confining pressure.

c) The effect of geogrid horizontal position on the tensile force propagations along the geogrid and vertical displacements

The effect of horizontal distance between center of footing and right edge of geogrid (SH) (i.e., 250 mm, 150 mm, 100 mm and 50 mm (Fig. 3) on the tensile force propagations along the geogrids and vertical displacements were analyzed. The number of geogrids was 1. The spacing between geogrid and footing was 40mm. The quantitative tensile force propagations along the geogrids were provided, as shown in Fig. 14. For each geogrid position, the maximum tensile force is found below the strip footing and the value decreases from the axisymmetric line to the both sides of the geogrid. The tensile force propagations along the geogrids have minimum value when the geogrid was situated in asymmetric line.

Fig. 15, shows the impact of geogrid position on the settlement of the footing. Vertical displacements of footing in all geogrid position cases were compared; the settlement of the footing has minimum value when the geogrid was situated in asymmetric line.

Fig. 16, shows the effect of horizontal distance between geogrid and footing on the vertical displacement of the ground surface. When the horizontal distance between geogrid and footing was 50 mm, the maximum settlement was occurred below the footing.

d) The effect of geogrid thickness on the tensile force propagations along the geogrids and vertical displacements

The effect of geogrid thickness on the tensile force propagations along the geogrids and vertical displacements for geogrid spacing of 40 mm were analyzed i.e., 7 mm, 15 mm and 25 mm (Fig. 4). The number of geogrids was 1 (N=1). The tensile force propagations along the geogrids were provided, as shown in Fig. 17. For each geogrid thickness, the maximum tensile force is found under the strip footing and the value decreases from the axisymmetric line to the both sides of the geogrid. The tensile force propagations along the geogrids were decreased by increasing the geogrid thickness.

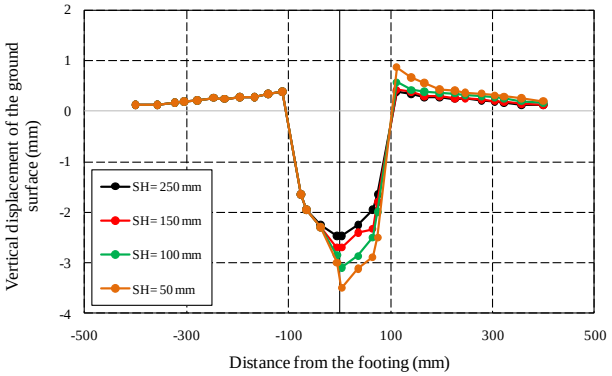

Fig. 16 Effect of horizontal distance between geogrid and the footing on the vertical displacement of the ground surface

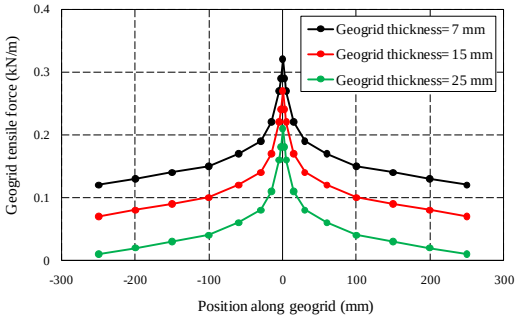

Fig. 17 Effect of geogrid thickness on the tensile force propagations along the geogrids

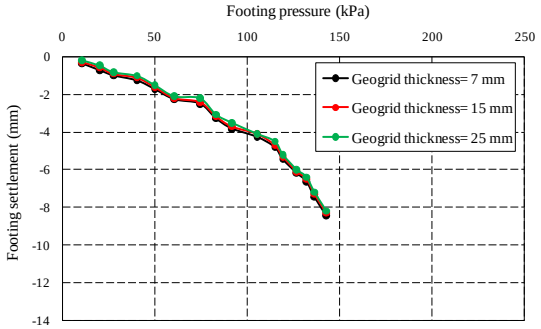

Fig. 18 Effect of geogrid thickness on the footing settlement

Fig. 18, shows the impact of geogrid thickness on the settlement of the footing. Vertical displacements along the geogrids in all geogrid thickness cases were compared, the settlement of the footing was decreased by increasing the geogrid thickness.

e) The effect of spacing between two geogrids and the footing on the tensile force propagations along the geogrid and vertical displacements

From above finding, it could be concluded that the best effectiveness spacing between one geogrid and footing was 40 mm. also the best position for geogrid was in axisymmetric line. In this stage, the spacing between upper geogrid and footing was kept constant, i.e., 40 mm, and the

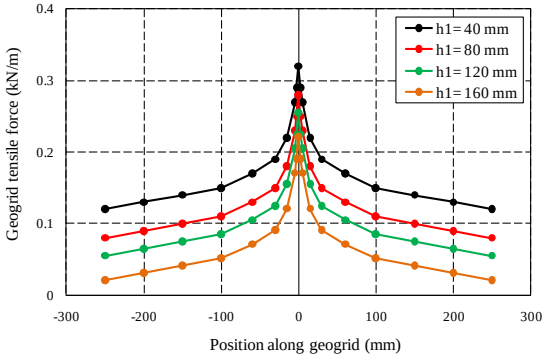

Fig. 19 Tensile force propagations along lower geogrid in reinforced soil samples

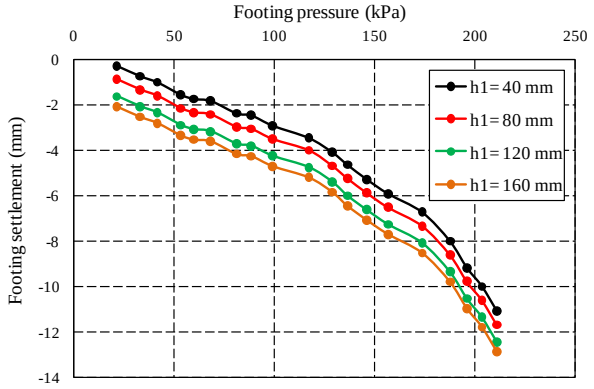

Fig. 20 Effect of geogrids spacing on the footing settlement

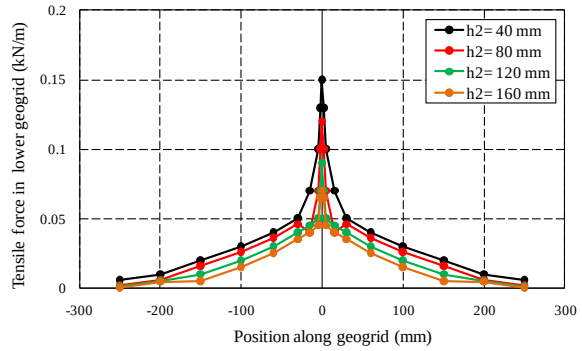

Fig. 21 Tensile force propagations along lower geogrid in reinforced soil samples

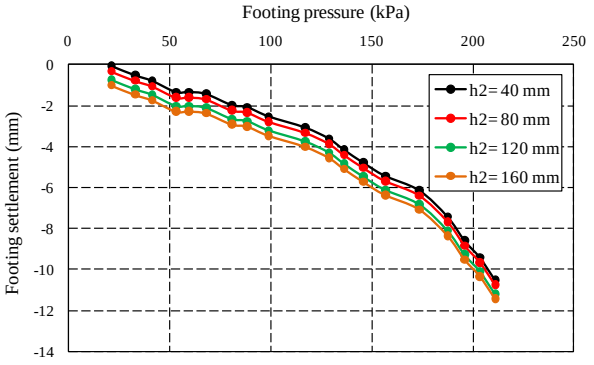

Fig. 22 Effect of geogrids spacing on the footing settlement

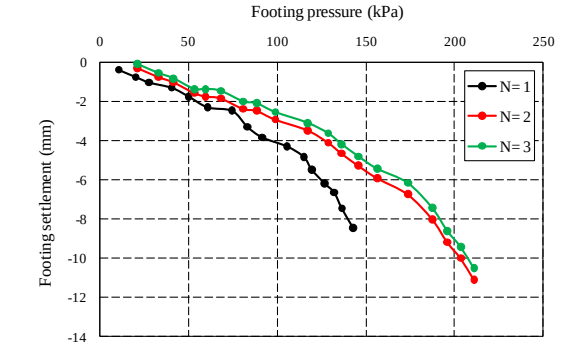

Fig. 23 Effect of geogrid number on the footing settlement

spacing between lower geogrid and upper geogrid were 40 mm, 80 mm, 120 mm and 160 mm (Fig. 5). The tensile force propagations along the lower geogrids were obtained, as shown in Fig. 19. For each geogrid layer, the maximum tensile force is found below the strip footing and the value decreases from the axisymmetric line to the both sides of the geogrid. The tensile force propagations along the geogrids were decreased by increasing the geogrids spacing.

Fig. 20, shows the effect of geogrids spacing on the footing settlement. Settlement of the footing in all cases were compared, the settlement of the footing was increased by increasing the geogrids spacing.

f) The effect of spacing between three geogrids and the footing on the tensile force along the geogrid and vertical displacements

From above finding, it could be concluded that the best effectiveness spacing between two geogrid was 40 mm. In this stage, the spacing between two geogrids and the footing was kept constant, i.e., 40 mm, and the spacing between lower geogrid and middle geogrid were 40 mm, 80 mm, 120 mm and 160 mm (Fig. 6). The tensile force propagations along the lower geogrids were obtained, as shown in Fig. 21. For each geogrid layer, the maximum tensile force is found below the strip footing and the value decreases from the axisymmetric line to the both sides of the geogrid. The tensile force propagations along the geogrids were decreased by increasing the geogrids spacing.

Fig. 22, shows the impacts of geogrids spacing on the vertical displacements of footing. Vertical displacements of footing in all cases were compared, the vertical displacement of the footing was increased by increasing the geogrids spacing.

g) The effect of geogrid number on the geogrid and footing settlement

Fig. 23, shows the effect of the footing pressure on the footing settlement for three various combinations of geogrid, i.e., one geogrid, two geogrid and three geogrids. The spacing between geogrids was 40 mm. the footing settlement was decreased by increasing the geogrid number.

3.2 Numerical modeling of tunnel reinforced by geogrid

In this research, DE modeling using PFC 2D was selected to examine the mechanisms of geogrid reinforcement in soil tunnel, that also were loaded with surface strip footings. In DEM examinations, the models and micro input factors footing particles, geogrids, soil particle, boundary walls and coffining pressure (0.001 MPa) were similar to using parameters in the numerical modelling of unreinforced and geogrid reinforced soil foundations. Fig. 24, depicts the soil tunnel loaded with a surface strip footing. The numerical strip footing had a width of 100 mm. Dimensions of rectangular tunnel was 200 mm×150 mm. This tunnel was supported by clump model with thickness 0f 15 mm. model dimension was 1000 m×600 mm. The

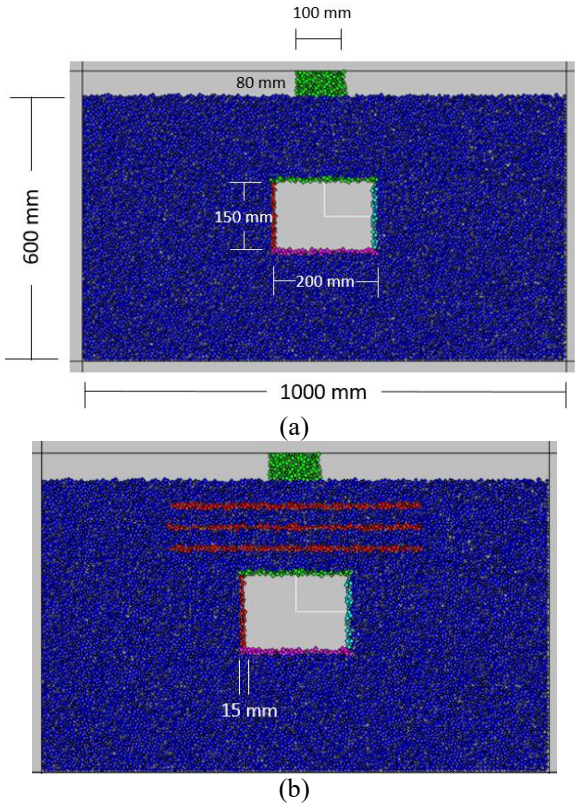

Fig. 24 Soil-tunnel loaded with a surface strip footing, (a) without geogrid and (b) with geogrid (N=3)

DEM examinations in this research emphasized on two cases: unreinforced (N=0 in Fig. 24(a)), and reinforced with three geogrid layers (N=3 in Fig. 24(b)), with the length of each geogrid 500 mm under confining pressure of 0.001 MPa. Each numerical sample was provided with multilayers, and when the ratio of the maximum unbalanced force to the maximum contact force in the sample decreased below 0.001, the equilibrium state of each soil layer was established. For the reinforced case, the geogrids with thickness 0f 15 mm were placed 40 mm, 80 mm and 120 mm beneath the footing base, respectively, as shown in Figure 24b. After the preparation of the final soil layer in the model, to model the strip footing, a set of bonded particles were produced on the top surface of the ground.

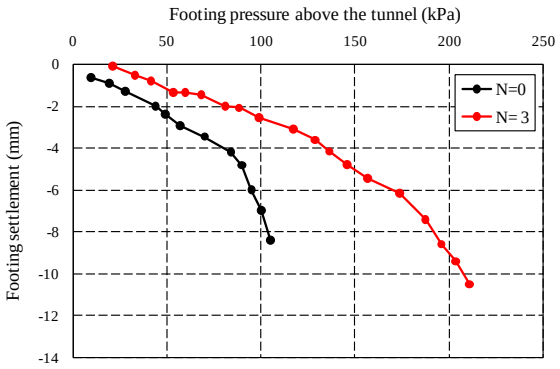

Fig. 25 Numerically obtained pressure–settlement relationships of the strip footings on the soil with and without geogrid reinforcement

A 10 kPa increase of vertical pressure directly applied to the bonded particles till the numerical samples failed. For each loading step, when the ratio of the maximum unbalanced force to the maximum contact force in the sample fell below 0.001, the equilibrium state of each soil layer was established. In the process of loading the applied vertical pressure, and the subsequent footing settlement at the equilibrium state of each loading step were recorded. In addition, the tensile forces and vertical displacements along the geogrids of the geogrid reinforced sample were recorded.

3.2.1 Numerical simulation results

Fig. 25, shows the numerically obtained pressure–settlement relationships of the strip footings on the soil with and without geogrid reinforcement. The bearing capacity of the strip footing with three layers of geogrids in comparison with the unreinforced type showed a significant increase. Such a great increase in the bearing capacity indicates the reinforcing impacts of geogrids on soil tunnel.

(a) Force propagations in soil and along geogrids

Figs. 26(a) and 26(b), depicts the contact force propagations in the soil and the qualitative tensile force propagations along the geogrids in the unreinforced and reinforced soil under a footing failure pressure of 110 kPa, which was the final bearing capacity of the unreinforced tunnel. The black and red lines indicate the contact shear and tensile forces inside the soil, while the horizontal red lines under the footing represent the tensile forces inside the geogrids. The thickness of the lines is depending on the magnitude of the contact forces and the tensile forces. Like the researches of DEM in reinforced soil foundations, big contact forces progressed under the strip footing.

In the unreinforced type (N=0), the contact forces symmetrically propagate along the vertical center of the strip footing. In the reinforced type (N=3), due to the activation of tensile forces inside the geogrids, the contact forces under the strip footing propagate nearly symmetrically along the vertical center of the strip footing. Furthermore, the activated geogrids act to extend the contact force dispensation in the reinforced soil. These DEM simulation results visualize the load distribution due to the load transfer between the soil and geogrids. Furthermore, of above qualitative force propagations in Fig. 26, quantitative tensile force propagations along the geogrids are provided too, as shown in Fig. 27 For each geogrid layer, the maximum tensile force within the geogrid is determined under the strip footing and the value decreases from the vertical center of the strip footing to both ends of the geogrids. below the strip footing, the tensile forces inside the upper geogrid compared to those inside the lower geogrids are greater.

b) Displacement propagations of soil particles and geogrids

Fig. 28, depicts the qualitative displacement propagations of soil particles in the unreinforced and reinforced soil under a footing pressure of 110 kPa. It can

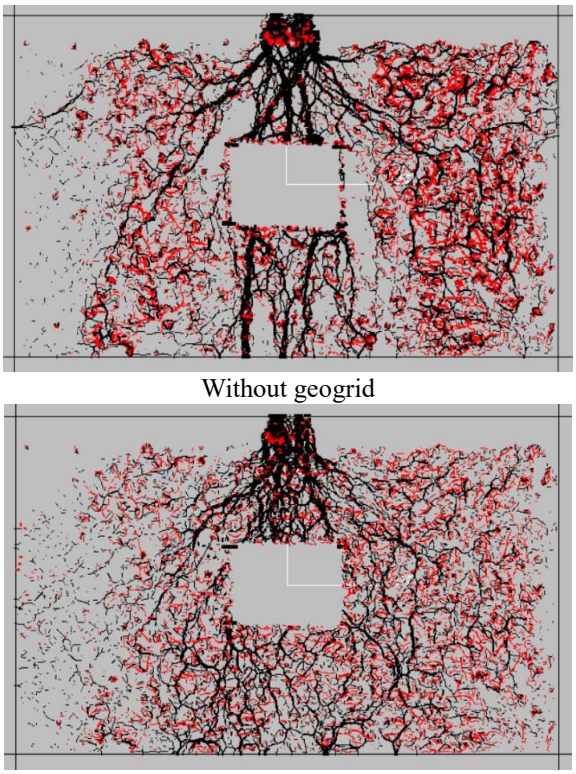

Fig. 26 Contact force propagations in soil tunnel and tensile force propagations along geogrids without and with geogrid reinforcement under identical loading state

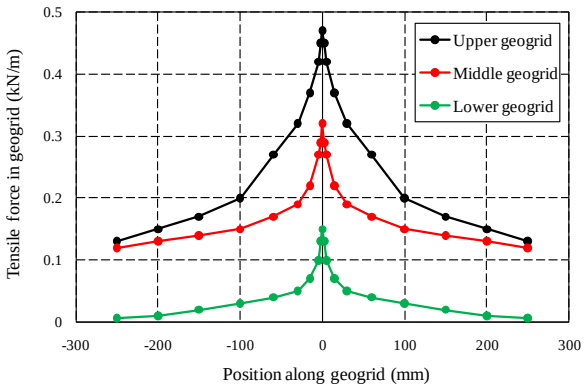

Fig. 27 Tensile force propagations along geogrid in reinforced soil

be concluded from Fig. 28(a) that a general shear failure mode happens in the unreinforced slope (N=0) and a sliding surface develops from the strip footing to the toe of the unreinforced soil. In the reinforced soil (N=3), the displacements of soil particles are restrained by the geogrids and, therefore, they are greatly smaller than those in the type of N=0. Furthermore, due to the load propagation the reinforced soil structure didn't experience any real slip surface developing. Big displacements of soil particles are just seen below the strip footing and above the upper geogrid, as shown in Fig. 28(b).

Fig. 29, shows the vertical displacements of the geogrids in the reinforced soil below a footing pressure of 110 kPa.

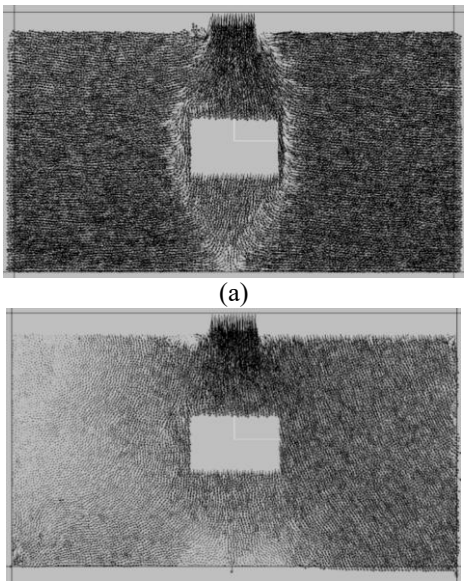

Fig. 28 Displacement propagations of soil particles in the unreinforced and reinforced soil below a footing pressure of 110 kPa

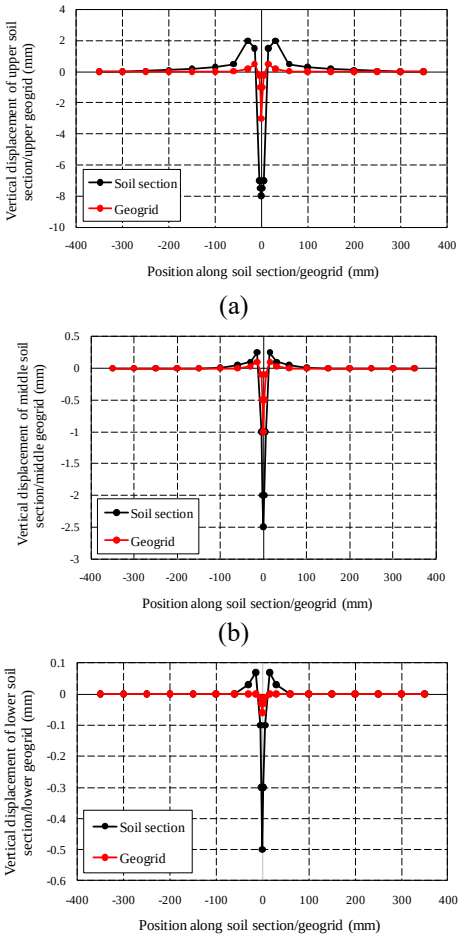

Fig. 29 Vertical displacement propagations along soil layer/geogrid in unreinforced and reinforced soil tunnel (a) upper geogrid, (b) middle geogrid and (c) lower geogrid

The vertical displacements of soil particles in horizontal parts of the unreinforced soil as a comparison are plotted in Fig. 29. The depths of geogrids in the reinforced soil are identical to the depths of the soil horizontal parts in the unreinforced soil. Below the strip footing, the maximum vertical displacement happens at the upper soil section, followed by the upper geogrid layer. Under the strip footing, the vertical displacements of the lower soil section and the lower geogrid are the smallest. Outside the range of the strip footing, the soil particles in the upper section have been forced aside, which compared to the soil particles beneath the strip footing, causes to the movement of soil particles in an opposite direction. The vertical displacements of geogrids outside the range of the strip footing are relatively small.

4. Conclusions

Discrete element modeling of unreinforced and geogrid reinforced soil foundations and was performed under surface strip footing loads. The influence of horizontal position of geogrid, vertical position, thickness, number, confining pressure have been examined on the footing settlement and tensile force propagations along the geogrids. Also, the interaction between rectangular tunnel and strip footing with and without presence of geogrid has been analyzed.

- The tensile force propagations along the geogrids were decreased by increasing the geogrid spacing. The vertical displacement of the footing was increased by increasing the geogrid spacing.
- The tensile force propagations along the geogrids were decreased by increasing the confining pressure. The settlement of the footing was decreased by increasing the confining pressure.
- The tensile force propagations along the geogrids were decreased by increasing the geogrid thickness. By increasing the geogrid thickness the vertical displacement of the footing was decreased.
- The tensile force propagations along the geogrids have minimum value when the geogrid was situated in asymmetric line. The settlement of the footing has minimum value when the geogrid was situated in asymmetric line.
- When the horizontal distance between geogrid and footing was 50 mm, the maximum settlement was occurred below the footing.
- The tensile force propagations along the geogrids were decreased by increasing the geogrids spacing. The vertical displacement of the footing was increased by increasing the geogrids spacing.
- The footing settlement was decreased by increasing the geogrid number. As the geogrid layers numbers increased, the bearing capacity of the soil foundations was greatly increased too.
- In the numerical modelling of unreinforced and reinforced soil tunnel, the bearing capacity of the reinforced soil tunnel was greatly increased due to the collaboration of three layers of geogrid reinforcements.

References

Adiyaman, G., Yaylacı, M. and Birinci, A. (2015), "Analytical and finite element solution of a receding contact problem", *Struct. Eng. Mech.*, **54**(1), 69-85. https://doi.org/10.12989/sem.2015.54.1.069.

Allen, T.M. and Bathurst, R.J. (2018), "Application of the simplified stiff-ness method to design of reinforced soil walls", *J. Geotech. Geoenviron. Eng.*, **144**(5), 04018024. https://doi.org/10.1061/(ASCE)GT.1943-5606.0001874.

Bathurst, R.J. and Javankhoshdel, S. (2017a), "Influence of model type, biasand input parameter variability on reliability analysis for simple limitstates in soil-structure interaction problems", *Georisk*, **11**(1). 42-54. https://doi.org/10.1080/17499518.2016.1154160

Bathurst, R.J., Javankhoshdel, S. and Allen, T.M. (2017b), "LRFD calibra-tion of simple soil-structure limit states considering method bias anddesign parameter variability", *J. Geotech. Geoenviron. Eng.*, **143**(9), 04017053. https://doi.org/10.1061/(ASCE)GT.1943-5606.0001735.

Bathurst, R.J., Lin, P. and Allen, T.M. (2019), "Reliability-based designof internal limit states for mechanically stabilized earth walls usinggeosynthetic reinforcement", *Can Geotech. J.,* **56**(6), 774-788. https://doi.org/10.1139/cgj-2018-0074.

Biabani, M.M., Ngo, N.T. and Indraratna B. (2016), "Performance evaluation of railway subballast stabilised with geocell based on pull-out testing", *Geotext. Geomembranes*, **44**(4), 579-591. https://doi.org/10.1016/j.geotexmem.2016.03.006

Brown, S.F., Kwan, J. and Thom, N.H. (2007), "Identifying the key parameters that influence geogrid reinforcement of railway ballast", *Geotext. Geomembranes*, **25**(6), 326-335. https://doi.org/10.1016/j.geotexmem.2007.06.003.

Chen, C., Mcdowell, G. and Rui, R. (2018), "Discrete element modelling of geogrids with square and triangular apertures", *Geomech. Eng.*, **16**(5), 495-501. http://doi.org/10.12989/gae.2018.16.5.495.

Chen, Q. (2007), "An Experimental Study on Characteristics and Behavior of Reinforced Soil Foundation", Ph.D. thesis. Louisiana State University, USA.

Choudhary, A.K. and Krishna, A.M. (2016), "Experimental investigation of interface behaviour of different types of granular soil/geosynthetics", *Int. J. Geosynth. Ground Eng.*, **2**(1) 11. https://doi.org/10.1007/s40891-016-0044-8.

Das, B.M., Shin, E.C. and Omar, M.T. (1994), "The bearing capacity of surface strip foundations on geogrid-reinforced sand clay- a comparative study", *Geotech. Geol. Eng.*, **12**(1), 1-14. https://doi.org/10.1007/BF00425933.

Demir, A., Yildiz, A., Laman, M. and Ornek, M. (2014), "Experimental and numerical analyses of circular footing on geogrid-reinforced granular fill underlain by soft clay", *Acta Geotech.*, **9**(4), 711-723. https://doi.org/10.1007/s11440-013-0207-x.

Dong, T., Cao, P. and Lin, Q. (2020), "Size effect on mechanical properties of rock-Like materials with three joints", *Geotech. Geol. Eng.*, **38**(11), 66-77. https://doi.org/10.1007/s43452-020-00027-z.

Dong, Y.L., Han, J. and Bai, X.H. (2011), "Numerical analysis of tensile behavior of geogrids with rectangular and triangular apertures", *Geotext. Geomembranes*, **29**(2), 83-91. https://doi.org/10.1016/j.geotexmem.2010.10.007.

Esmaeili, M., Zakeri, J.A. and Babaei, M. (2017), "Laboratory and field investigation of the effect of geogrid-reinforced ballast on railway track lateral resistance", *Geotext. Geomembranes*, **45**(2), 23-33. https://doi.org/10.1016/j.geotexmem.2016.11.003.

Gao, G. and Meguid, M.A. (2018), "Effect of particle shape on the response of geogrid-reinforced systems: insights from 3D discrete element analysis", *Geotext. Geomembranes*, **46**(1), 685-

698. https://doi.org/10.1016/j.geotexmem.2018.07.001.
Gu, F., Luo, X. and Luo, R. (2016), "Numerical modeling of geogrid-reinforced flexible pavement and corresponding validation using large-scale tank test", *Constr. Build. Mater*., **122**, 214-230. https://doi.org/10.1016/j.conbuildmat.2016.06.081.
Gutierrez, M., Muftah, A. (2015), "Micro and Macro Behavior of Granular Materials in Simple Shear", *Crc Press-Taylor & Francis Group, Boca Raton*., 91-96. DOI: 10.1201/b17395-15
Han, B.Y., Ling, J.M. and Shu, X. (2018), "Laboratory investigation of particle size effects on the shear behavior of aggregate-geogrid interface", *Constr. Build. Mater*., **158**, 1015-1025. https://doi.org/10.1016/j.conbuildmat.2017.10.045.
Huang, C.C. and Tatsuoka, F. (1990), "Bearing capacity of reinforced horizontal sandy ground", *Geotext. Geomembranes*, **9**(1), 51-82. https://doi.org/10.1016/0266-1144(90)90005-W.
Indraratna, B. and Rujikiatkamjorn, C. (2011), "Behavior of geogridreinforced ballast under various levels of fouling", *Geotext. Geomembranes*, **29**(3), 313-322. https://doi.org/10.1016/j.geotexmem.2011.01.015.
Indraratna, B., Hussaini, S.K.K. and Vinod, J.S. (2012), "On The Shear Behavior of Ballast-Geosynthetic Interfaces", *Geotech. Test. J.*, **35**(2), 305-312. https://doi.org/10.1520/GTJ103317.
Indraratna, B., Hussaini, S.K.K. and Vinod, J.S. (2013), "The lateral displacement response of geogrid-reinforced ballast under cyclic loading", *Geotext. Geomembranes*, **39**, 20-29. https://doi.org/10.1016/j.geotexmem.2013.07.007.
Khing, K.H., Das, B.M., Puri, V.K., Cook, E.E. and Yen, S.C. (1993), "The bearing-capacity of a strip foundation on geogrid-reinforced sand", *Geotext. Geomembranes*, **12**(4), 351-361. https://doi.org/10.1016/0266-1144(93)90009-D.
Kim, D. (2020), "Determination of effective parameters on surface settlement during shield TBM", *Geomech. Eng*., **21**(2), 56-72. https://doi.org/10.12989/gae.2020.21.2.153.
Lin Q. and Cao, P. (2021b), "Crack coalescence in rock-like specimens with two dissimilar layers and pre-existing double parallel joints under uniaxial compression", *Int. J. Rock Mech. Min. Sci.*, **139**(8), 98-105. https://doi.org/10.1016/j.ijrmms.2021.104621.
Lin, P. and Bathurst, R.J. (2018a), "Influence of cross-correlation betweennominal load and resistance on reliability-based design for simple linearsoil-structure limit states", *Can. Geotech. J*., **55**, (2), 279-295. https://doi.org/10.1139/cgj-2017-0012.
Lin, P. and Bathurst, R.J. (2018b), "Reliability-based internal limit statesanalysis and design of soil nails using different load and resistancemodels", *J. Geotech. Geoenviron. Eng*., **144**(5), 04018022. https://doi.org/10.1061/(ASCE)GT.1943-5606.0001862.
Lin, Q. and Cao, P. (2020), "Strength and failure characteristics of jointed rock mass with double", *Theor. Appl. Fract. Mech.*, **109**(7), 45-61. https://doi.org/10.1016/j.tafmec.2020.102692.
Lin, Q. and Cao, P. (2021a), "Mechanical behavior of a jointed rock mass with a circular hole under compression-shear loading: Experimental and numerical studies", *Theor. Appl. Fract. Mech.*, **114**(4), 45-67. https://doi.org/10.1016/j.tafmec.2021.102998.
Lu, M. a nd Mcdowell, G.R. (2006), "The importance of modelling ballast particle shape in the discrete element method", *Granular. Matter.,* **9**(1-2) 69-80. https://doi.org/10.1007/s10035-006-0021-3.
Luat, N. (2020), "Application of artificial neural networks in settlement prediction of shallow foundations on sandy soils". *Geomech. Eng*., **20**(5), 33-45. http://doi.org/10.12989/gae.2020.20.5.385.
Mcdowell, G.R. and Harireche, O. (2002), "Discrete element modelling of soil particle fracture", *Geotechnique*, **52**(2), 131-135. https://doi.org/10.1680/geot.2002.52.2.131.
Mcdowell, G.R., Harireche, O. and Konietzky, H. (2006), "Discrete element modelling of geogrid-reinforced aggregates". *Proceedings of the Institution of Civil Engineers-Geotechnical Engineering*, **159**(1), 35-48. https://doi.org/10.1680/geng.2006.159.1.35.
Miao, C.X., Zheng, J.J. and Zhang, R.J. (2017), "Visualization of pullout behaviour of geogrid in sand with emphasis on size effect of protrusive junctions", *J. Central South Univ*., **24**(9), 2121-2133. https://doi.org/10.1007/s11771-017-3621-7.
Miao, C.X., Zheng, J.J., Zhang, R.J. and Cui, L. (2017), "DEM modeling of pullout behavior of geogrid reinforced ballast: the effect of particle shape", *Comput. Geotech*., **81**, 249-261. https://doi.org/10.1016/j.compgeo.2016.08.028.
Moradi, G.H. (2019), "Small- and large-scale analysis of bearing capacity and load-settlement behavior of rock-soil slopes reinforced with geogrid-box method", *Geomech. Eng*., **18**(3), 123-138. https://doi.org/10.12989/gae.2019.18.3.315.
Ngo, N.T., Indraratna, B. and Rujikiatkamjorn, C. (2014), "DEM simulation of the behaviour of geogrid stabilised ballast fouled with coal", *Comput. Geotech*. **55**, 224-231. https://doi.org/10.1016/j.compgeo.2013.09.008.
Ngo, N.T., Indraratna, B. and Rujikiatkamjorn, C. (2016), "Modelling geogrid-reinforced railway ballast using the discrete element method", *Transp. Geotech*., **8**, 86-102. https://doi.org/10.1016/j.trgeo.2016.04.005.
Ngo, N.T., Indraratna, B. and Rujikiatkamjorn, C. (2017), "A study of the geogrid–subballast interface via experimental evaluation and discrete element modelling", *Granular Matter.*, **19**(3), 54. https://doi.org/10.1007/s10035-017-0743-4.
Nimbalkar, S., Neville, T. and Indraratna, B. (2014), "Performance assessment of reinforced ballasted rail track", *Proceedings of the ICE - Ground Improvement*, **167**(1), 24-34. https://doi.org/10.1680/grim.13.00018.
Öner E., Yaylaci, M. and Birinci, A. (2015), "Analytical solution of a contact problem and comparison with the results from FEM", *Struct. Eng. Mech.*, **54**(4), 607-622. https://doi.org/10.12989/sem.2015.54.4.607.
Qian, Y., Tutumluer, E. and Mishra, D. (2018), "Triaxial testing and discrete-element modelling of geogrid-stabilised rail ballast", *Proceedings of the Institution of Civil Engineers-Ground Improvement,* **171**(4), 223–231. https://doi.org/10.1680/jgrim.17.00068.
Rezaei, A.H. (2019), "EPB tunneling in cohesionless soils: A study on Tabriz Metro settlements", *Geomech. Eng*., **19**(2), 89-99. https://doi.org/10.12989/gae.2019.19.2.153.
Sweta, K. and Hussaini, S.K.K. (2019), "Performance of the geogrid-reinforced railroad ballast in direct shear mode". *Proceedings of the Institution of Civil Engineers. Ground Improvement*, **172**(4), 244-256. https://doi.org/10.1680/jgrim.18.00107.
Teixeira, S.H.C., Bueno, B.S. and Zornberg, J.G. (2007), "Pullout resistance of individual longitudinal and transverse geogrid ribs", *J. Geotech. Geoenviron. Eng*., **133**(1), 37-50. https://doi.org/10.1061/(ASCE)1090-0241(2007)133:1(37).
Thornton, C. (2000), "Numerical simulations of deviatoric shear deformation of granular media", *Geotechnique*, **50**(1), 43-53. https://doi.org/10.1680/geot.2000.50.1.43.
Tran, V.D.H., Meguid, M.A. and Chouinard, L.E. (2015), "Three-dimensional analysis of geogrid- reinforced soil using a finite-discrete element framework", *Int. J. Geomech.*, **15**(4), 04014066. https://doi.org/10.1061/(ASCE)GM.1943-5622.0000410.
Uzun Yaylacı, E., Yaylacı, M., Ölmez, H. and Birinci, A. (2020), "Artificial neural network calculations for a receding contact problem", *Comput. Concrete*, **25**(6), 551-563 https://doi.org/10.12989/cac.2020.25.6.551.
Wang, Z. and Jacobs, F. (2020), "Visualisation and quantification of geogrid reinforcing effects under strip footing loads using

discrete element method", *Geotext. Geomembranes*, **48**, 62-70. https://doi.org/10.1016/j.geotexmem.2019.103505.
Wang, Z., Jacobs, F. and Ziegler, M. (2014), "Visualization of load transfer behaviour between geogrid and sand using PFC2D", *Geotext. Geomembranes*, **42**(2), 83-90. https://doi.org/10.1016/j.geotexmem.2014.01.001.
Wang, Z., Jacobs, F. and Ziegler, M. (2016), "Experimental and DEM investigation of geogridsoil interaction under pullout loads". *Geotext. Geomembranes*, **44**(3), 230-246. https://doi.org/10.1016/j.geotexmem.2015.11.001.
Yang, G. and Liu, H. (2012), "Geogrid-reinforced lime-treated cohesive soil retaining wall: case study and implications", *Geotext. Geomembranes*, **35**, 112-118. https://doi.org/10.1016/j.geotexmem.2012.09.001.
Yang, X.L. (2018), "Catastrophe analysis of active-passive mechanisms for shallow tunnels with settlement", *Geomech. Eng.*, **15**(1), 99-111. https://doi.org/10.12989/gae.2018.15.1.621.
Yaylaci M. and Birinci, A. (2013), "The receding contact problem of two elastic layers supported by two elastic quarter planes", *Struct. Eng. Mech.*, **48**(2), 241-255. https://doi.org/10.12989/sem.2013.48.2.241.
Yaylacı M., Adıyaman E., Öner E. and Birinci A., (2021a), "Investigation of continuous and discontinuous contact cases in the contact mechanics of graded materials using analytical method and FEM", *Comput. Concrete*, **27**(3), 199-210. https://doi.org/10.12989/cac.2021.27.3.199.
Yaylaci, M. (2016), "The investigation crack problem through numerical analysis", *Struct. Eng. Mech.*, **57**(6), 1143-1156. https://doi.org/10.12989/sem.2016.57.6.1143,
Yaylacı, M., Adıyaman, E., Öner, E. and Birinci, A., (2020), "Examination of analytical and finite element solutions regarding contact of a functionally graded layer", *Struct. Eng. Mech*., **23**(3), 21-34. https://doi.org/10.12989/sem.2020.76.3.325.
Yaylacı, M., Eyüboğlu, A., Adıyaman, G., Uzun Yaylacı, E., Öner, E. and Birinci, A. (2021b), "Assessment of different solution methods for receding contact problems in functionally graded layered mediums", *Mech. Mater.*, **15**(3), 77-88. https://doi.org/10.1016/j.mechmat.2020.103730.
Zhang, J., Zheng, J.J. and Chen, B.G. (2013), "Coupled mechanical and hydraulic modeling of a geosynthetic-reinforced and pile-supported embankment", *Comput. Geotech*., **52**, 28-37. https://doi.org/10.1016/j.compgeo.2013.03.003.
Zhao, X. and Evans, T.M. (2009), "Discrete simulations of laboratory loading conditions", *Int. J. Geomech*., **9**(4), 169-178. https://doi.org/10.1061/(ASCE)1532-3641(2009)9:4(169).

CC